

# Skillful multiyear predictions of ocean acidification in the California Current System

Riley X. Brady<sup>1\*</sup>, Nicole S. Lovenduski<sup>1</sup>, Stephen G. Yeager<sup>2</sup>, Matthew C. Long<sup>2</sup>, Keith Lindsay<sup>2</sup>

<sup>1</sup>Department of Atmospheric and Oceanic Sciences and Institute of Arctic and Alpine Research, University of Colorado, Boulder, Colorado, USA

<sup>2</sup>Climate and Global Dynamics Laboratory, National Center for Atmospheric Research, Boulder, Colorado, USA

\*Correspondence to: riley.brady@colorado.edu

1 **Abstract:** The California Current System (CCS) sustains economically valuable  
2 fisheries and is particularly vulnerable to ocean acidification, due to the natural  
3 upwelling of corrosive waters that affect ecosystem function. Marine resource managers  
4 in the CCS could benefit from advanced knowledge of ocean acidity on multiyear  
5 timescales. We use a novel suite of retrospective forecasts with an initialized Earth  
6 system model (ESM) to predict the evolution of surface pH anomalies in the CCS. Here  
7 we show that the forecast system skillfully predicts observed surface pH variations  
8 multiple years in advance over a naïve forecasting method. Skillful predictions of  
9 surface pH are mainly derived from the initialization of dissolved inorganic carbon  
10 anomalies that are subsequently transported into the CCS. Our results demonstrate the  
11 potential for ESMs to provide predictions relevant to managing the onset and impacts of  
12 ocean acidification in this vulnerable region.

13 Ocean acidification is an ongoing large-scale environmental problem, whereby  
14 the absorption of anthropogenic CO<sub>2</sub> by the ocean lowers its pH, impacting ocean  
15 ecosystems worldwide<sup>1</sup>. The California Current System (CCS) supports productive  
16 fisheries crucial to the US economy and is particularly vulnerable to ocean acidification  
17 due to the upwelling of naturally corrosive (*i.e.*, relatively low pH) waters to the surface<sup>2</sup>.  
18 The upwelling process results from equatorward winds along the western North  
19 American coastline. These winds facilitate both coastal upwelling and curl-driven Ekman  
20 suction, forcing waters enriched in carbon and nutrients from beneath the thermocline to  
21 the surface<sup>3</sup>. These nutrient subsidies drive high productivity in CCS waters, essential to  
22 supporting regional fisheries<sup>4</sup>. However, the upwelled waters are also corrosive due to  
23 their high content of remineralized carbon. The air-to-sea flux of anthropogenic CO<sub>2</sub> into  
24 the CCS further compounds this natural acidity. Multiple studies over the past decade  
25 have observed coastal CCS waters that are anomalously low in pH and undersaturated  
26 with respect to calcium carbonate minerals<sup>5-7</sup>. These conditions adversely affect a wide  
27 range of organisms that precipitate calcium carbonate shells, such as pteropods,  
28 coccolithophores, and shellfish<sup>1</sup>. These organisms are keystone species that support  
29 commercial and recreational fisheries which generate approximately \$6B in revenue per  
30 year<sup>8</sup>. The CCS's intersection between economically valuable fisheries and natural  
31 vulnerability to ocean acidification makes it a high-priority region to study for multiyear  
32 biogeochemical predictions. With advanced warning of regional pH declines, managers  
33 of shellfisheries could select for more favorable sites (*i.e.*, regions forecasted to have  
34 more basic conditions) or buffer specific coastal waters with sodium carbonate<sup>9</sup>.

35 **Results**

36 **Forecasting ocean biogeochemistry in the California Current**

37 Prediction efforts for the CCS have focused primarily on using seasonal forecasts of sea  
38 surface temperature<sup>10–12</sup> (SST) and biogeochemical variables<sup>13</sup> (*e.g.*, dissolved oxygen  
39 and bottom pH) as inputs into ecosystem forecasting models. A more recent effort  
40 demonstrates the potential for initialized predictions of surface chlorophyll in the CCS  
41 with two year forecasts<sup>14</sup>. However, no studies have attempted to predict ocean  
42 biogeochemistry in the CCS at the multiannual to decadal scale. This temporal scale is  
43 critical for fisheries managers, as it aids them in setting annual catch limits, changing  
44 and introducing closed areas, and adjusting quotas for internationally shared fish  
45 stocks<sup>15</sup>. However, decadal forecasting of ocean biogeochemistry is still in its infancy<sup>16–</sup>  
46 <sup>20</sup>. In the absence of biogeochemical predictions longer than nine months, managers  
47 rely upon the assumption that anomalies persist from year to year. These so-called  
48 persistence forecasts are commonly used as a baseline to put initialized skill into  
49 context and work at lead times commensurate with the decorrelation timescales of the  
50 system<sup>10–12,15</sup>. On the other hand, initialized predictions use a physically based  
51 modeling framework to advance information from initial conditions forward in time; if the  
52 system is predictable (*i.e.*, sufficiently deterministic) and the model skillful, this can yield  
53 a powerful forecasting framework. Recent ensemble simulations of initialized ESMs  
54 provide the most powerful tool currently available for improving upon decadal  
55 persistence forecasts. Their coupling of global physical models of the atmosphere,  
56 ocean, cryosphere, and land with the carbon cycle, terrestrial and marine ecosystems,

57 atmospheric chemistry, and natural and human disturbances allows one to deeply  
58 investigate how interactions between the physical climate system and biosphere lead to  
59 predictability in a complex system such as the CCS<sup>21</sup>. These predictions have the  
60 potential to improve upon the persistence management method, pushing the horizon of  
61 forecasting ecosystem stressors past a single season or year.

62 Here we use an initialized global ESM with embedded ocean biogeochemistry,  
63 the Community Earth System Model Decadal Prediction Large Ensemble<sup>22</sup> (CESM-  
64 DPLE), to make retrospective forecasts of surface pH anomalies in the CCS from 1955  
65 through 2017. The CESM-DPLE employs an ocean model with nominal 1° x 1°  
66 horizontal resolution and 60 vertical levels. Forty ensemble members were initialized  
67 annually on November 1<sup>st</sup> from a forced ocean-sea ice reconstruction (hereafter referred  
68 to as the “reconstruction”) and then the coupled simulations were integrated forward for  
69 ten years (Fig. 1, A and B; see methods and supplementary). The reconstruction is  
70 skillful in representing surface pH variability on seasonal to interannual timescales in the  
71 CCS (Fig. S1). Due to the diverse terminology used in weather and climate  
72 forecasting<sup>23</sup>, we are careful with our definitions. We use the phrase “potential  
73 predictability” when referring to correlations between CESM-DPLE and the  
74 reconstruction. High correlation coefficients (*i.e.*, high potential predictability) represent  
75 the theoretical upper limit for predictions in the real world, given the chaotic nature of  
76 the climate system<sup>24</sup>. We use the phrase “predictive skill” when comparing CESM-DPLE  
77 to observations; skill demonstrates our ability to predict the true evolution of the real  
78 world with CESM-DPLE. We quantify our ability to predict anomalies with the anomaly

79 correlation coefficient (ACC), and our accuracy in predicting anomaly magnitudes with  
80 the mean absolute error (MAE). We compare our initialized forecasts to a simple  
81 persistence forecast and the uninitialized CESM Large Ensemble<sup>25</sup> (CESM-LE) mean,  
82 which includes the same external forcing (*i.e.*, rising atmospheric CO<sub>2</sub>) as the CESM-  
83 DPLE. The former assesses whether CESM-DPLE is useful relative to a simple  
84 forecasting method, while the latter determines the degree to which initialization  
85 engenders predictability beyond that afforded by supplying the model with time-varying  
86 forcing. We test predictive skill by comparing the initialized forecasts to a gridded  
87 observational product of surface pH from the Japan Meteorological Agency (JMA),  
88 which spans 1990–2017<sup>26,27</sup>. This product is based upon empirical relationships derived  
89 for alkalinity and pCO<sub>2</sub> as functions of *in situ* measurements, such as SST and sea  
90 surface height, which were then used in a carbonate system solver to derive gridded  
91 surface pH (see methods). Our focus in this study is on surface pH anomalies within the  
92 California Current Large Marine Ecosystem (see Fig. 1C for the spatial domain). We  
93 remove a second-order trend from all surface pH time series, since the long-term ocean  
94 acidification signal dominates over the 1954–2017 period (Fig. 1A). We aim to test our

95 ability to predict year-to-year variations in CCS surface pH anomalies (Fig. 1B), which  
96 act to temporarily accelerate or slow down the ongoing ocean acidification problem.

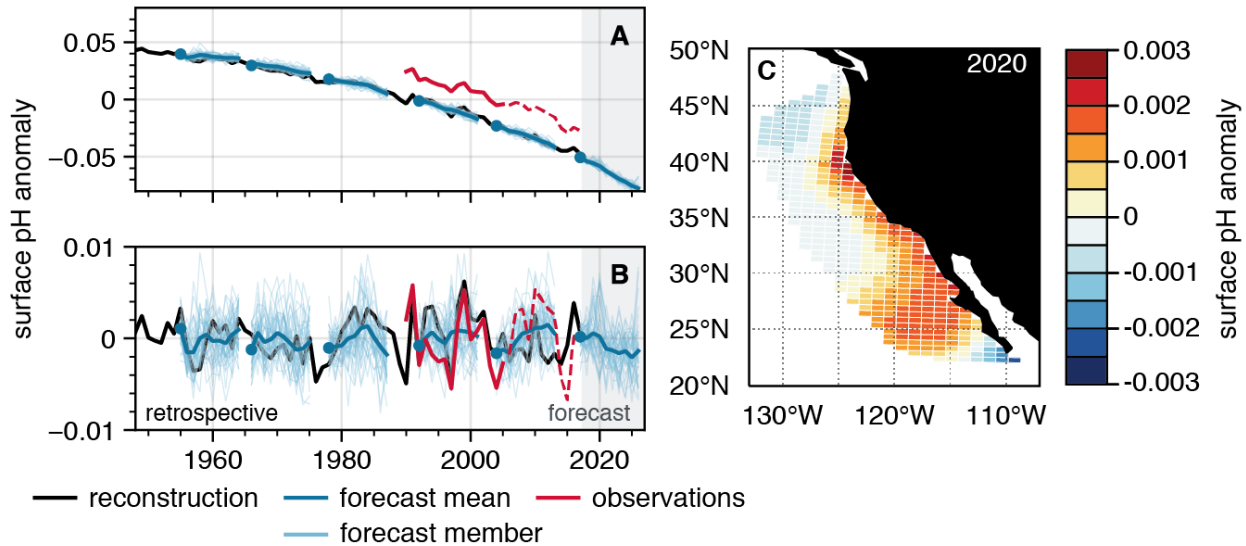


**Fig. 1.** *CESM-DPLE experimental design and near-future surface pH anomaly forecast.* (A) Trended and (B) detrended area-weighted annual surface pH anomalies for the (black) reconstruction, (red) observational product, and (blue) CESM-DPLE decadal forecasts initialized in 1954, 1965, 1977, 1991, 2003, and 2017 (other initializations were omitted for visual clarity). The dark blue line is the ensemble mean forecast, and thin blue lines are the individual 40 forecasts. The dashed red lines denote when the model loses observed variability in atmospheric CO<sub>2</sub> forcing (see Fig. S7A). (C) 2020 forecast for detrended surface pH anomalies in the CCS, based on the lead year 3 forecast initialized on November 1<sup>st</sup>, 2017. Positive values denote a basic anomaly (reduction in the ocean acidification trend), while negative values denote an acidic anomaly (acceleration of the ocean acidification trend).

## 97 Predictions of simulated and observed surface pH

98 Retrospective forecasts of detrended annual surface pH anomalies in the CCS suggest  
99 a potential to predict multiple years in advance over a simple persistence forecast (Figs.  
100 2 and 3). Although a persistence forecast is valuable at lead year one in parts of the  
101 CCS (Fig. 2F), the initialized forecast is statistically significant over persistence nearly  
102 everywhere (Fig. 2K). By lead year two, persistence begins to yield negative ACCs in

103 the southern portion of the CCS, while retaining some positive correlation in the north;  
104 ACCs become non-significant and weakly negative from lead year three and beyond  
105 (Fig. 2, H to J). The initialized forecast, in contrast, retains predictability in the central  
106 and southern CCS through lead year five (Fig. 2, A to E). Initialized predictions have  
107 higher ACCs than a persistence forecast everywhere out to five-year leads, save for  
108 three coastal grid cells along the coastal Pacific Northwest in lead year three (Fig. 2, K  
109 to O). An area-weighted perspective of the CCS reveals that the initialized forecast is  
110 significantly better than both persistence and the uninitialized forecast through five-year  
111 leads (Fig. 3A). The lead year one ACC of 0.72 explains over 50% of the variance in  
112 predicted surface pH anomalies and is comparable or better than the skill achieved by

113 seasonal forecasts of SSTs in the CCS<sup>10,11</sup>. The MAE is smaller than both persistence  
 114 and the uninitialized forecast over all ten lead years (Fig. 3B).

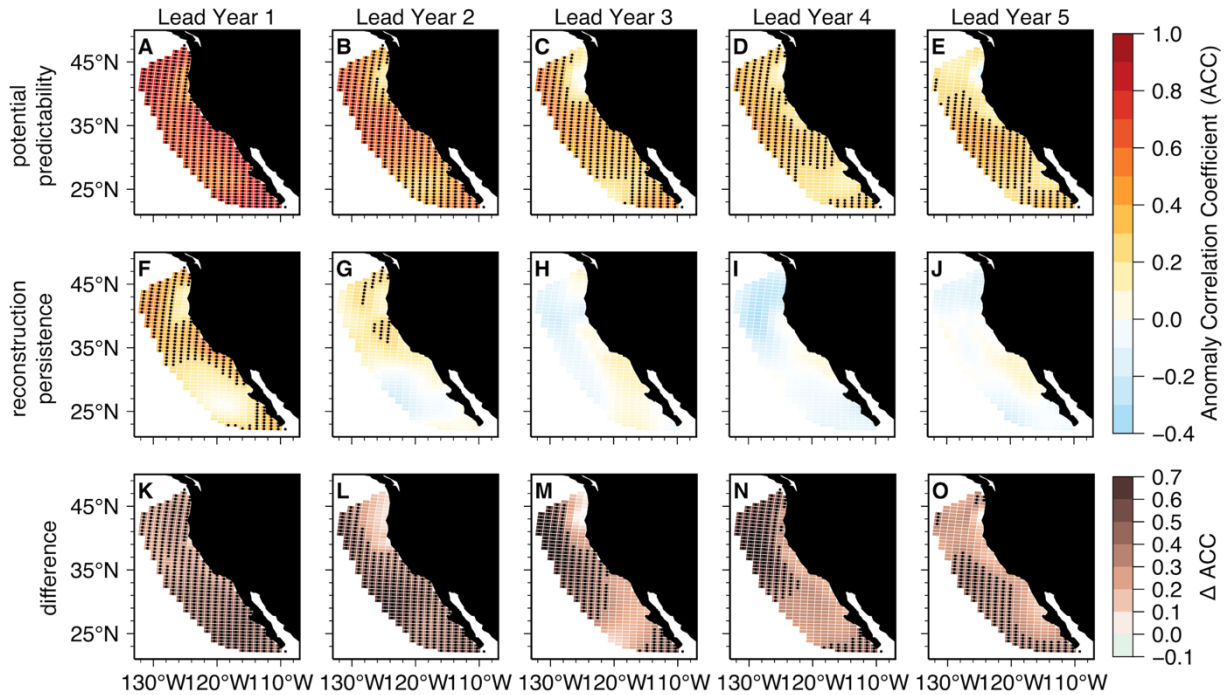


**Fig. 2.** Potential predictability of surface pH in the California Current. (A to E) CESM-DPLE initialized forecast of detrended annual surface pH anomalies for lead years one through five correlated with the reconstruction. (F to J) Persistence forecast for the reconstruction for lead years one through five. Stippling in A to J denotes statistically significant correlations at the 95% level using a *t* test. (K to O) Difference between the CESM-DPLE forecast ACCs and persistence. Stippling indicates that the initialized prediction is statistically significant over the persistence forecast at the 95% level using a *z* test. Only positive ACCs and  $\Delta$ ACCs are stippled.



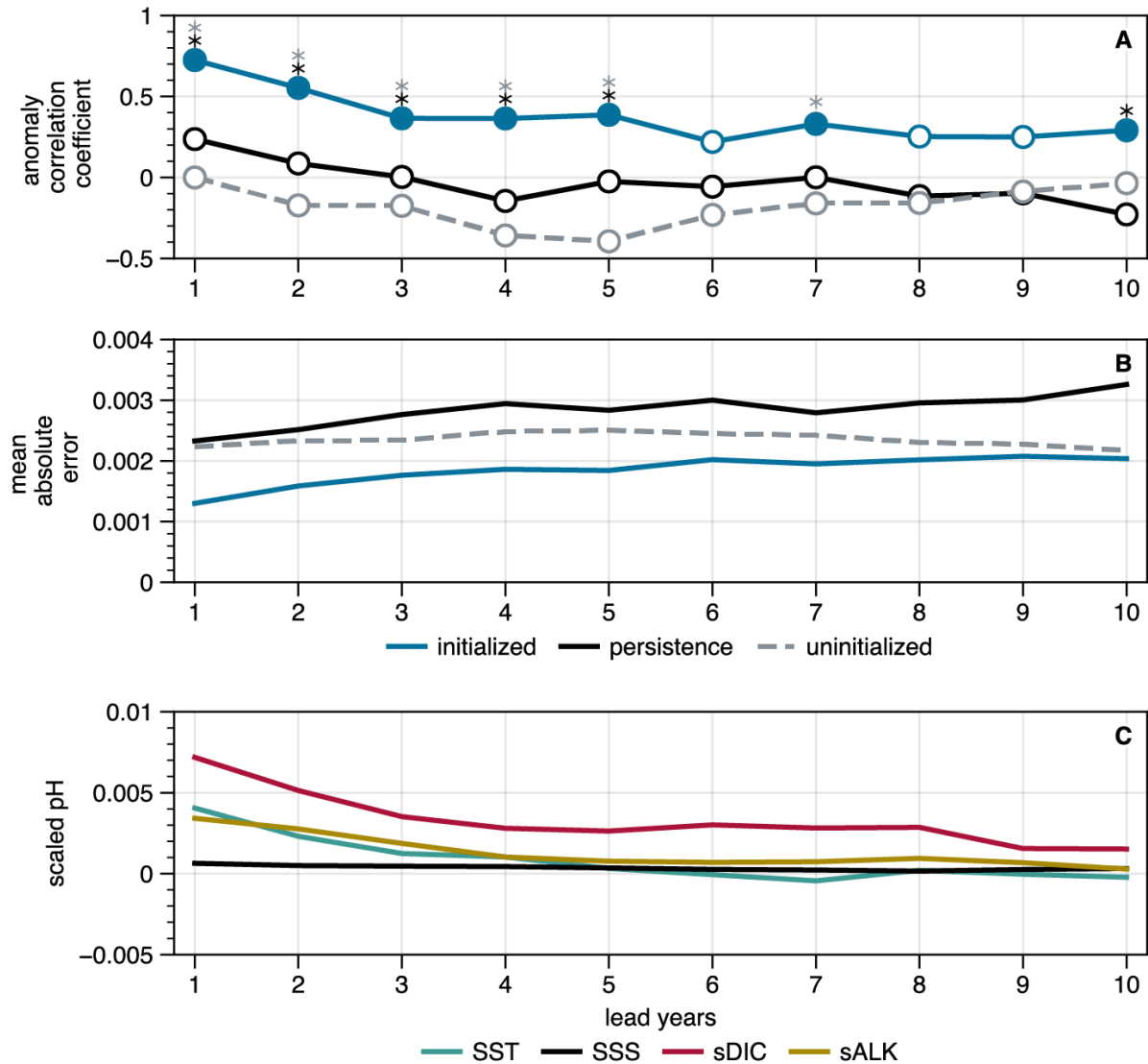


**Fig. 3.** Area-weighted potential predictability of surface pH in the California Current and driver variables of surface pH predictability. **(A)** ACCs for ten lead years for (blue) CESM-DPLE, (black) a persistence forecast from the reconstruction, and (grey) the uninitialized CSM-LE. Filled circles denote statistically significant positive correlations at the 95% level using a *t* test. Black and gray asterisks indicate significant predictability over persistence and the uninitialized forecast at the 95% level using a *z* test, respectively. **(B)** As in **(A)**, but for MAE and without significance testing. **(C)** Scaled predictability in common pH units (see supplementary methods) of (black) sea surface salinity, (teal) sea surface temperature, (gold) salinity-normalized alkalinity, and (red) salinity-normalized dissolved inorganic carbon.

115 Because the reconstruction simulates the mean state, seasonal cycle, and

116 variability of surface pH in the CCS well (Figs. S1 and S2), potential predictability

117 extends to predictive skill relative to the observational product (Fig. 4). Initialized  
118 predictions have positive ACCs throughout the CCS at lead year one (Fig. 4A), and  
119 have significant skill over persistence through lead year four from Cape Mendocino to  
120 Baja California (Fig. 4, K to N). Persistence in the observationally based surface pH  
121 estimates is somewhat useful south of Cape Mendocino at lead year one, but yields  
122 negative ACCs from lead years two to five throughout most of the CCS (Fig. 4, F to J).  
123 Note, however, that virtually none of these correlations are statistically significant.  
124 Across all five lead years, ACCs from the initialized predictions are larger than those of  
125 observational persistence for most of the CCS (Fig. 4, K to O), with an area-weighted  
126 mean  $\Delta$ ACC ranging from 0.17 to 0.48. Skill is lost for the southernmost portion of the  
127 CCS by lead year two (Fig. 4B), followed by the Pacific Northwest at lead year three  
128 (Fig. 4C). Bias in the initialized predictions of the observational surface pH (as  
129 measured by the MAE) are smaller than that of observational persistence for most of  
130 the CCS over five lead years (Fig. S5). Our results suggest that CESM-DPLE could be  
131 used for multiyear forecasting of surface pH variability in the CCS today. Fig. 1C shows  
132 the forecast of surface pH anomalies in the CCS for 2020, which corresponds to a lead  
133 year three forecast from the November 1<sup>st</sup>, 2017 initialization of CESM-DPLE. Our  
134 forecast suggests that variability in surface pH will reduce the ocean acidification trend  
135 along the coastline and in the southern CCS, but will slightly enhance the trend offshore  
136 in the central and northern CCS.

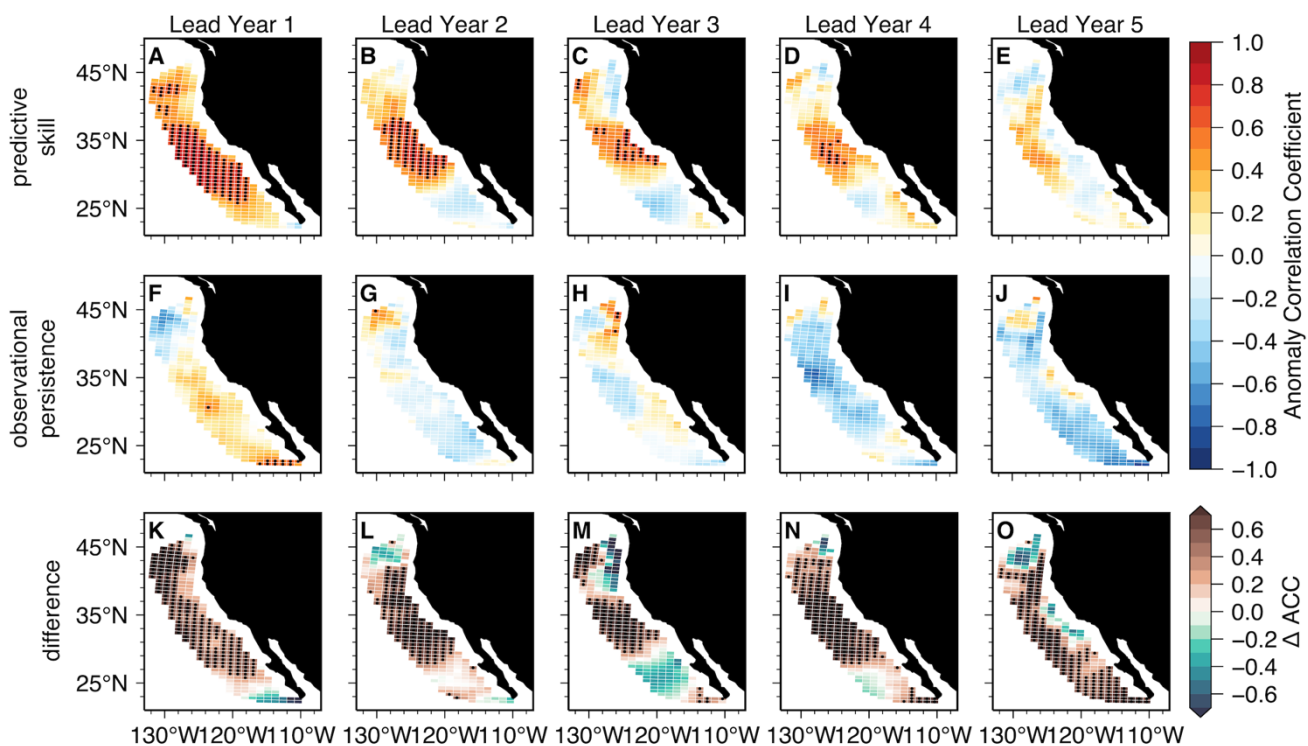


**Fig. 4.** *Predictive skill of surface pH anomalies in the California Current.* (A to E) CESM-DPLE initialized forecast of detrended annual surface pH anomalies for lead years one through five correlated with the observational product over 1990–2005. (F to J) Persistence forecast for the observations for lead years one through five. Stippling in A to J denotes statistically significant correlations at the 95% level using a *t* test. (K to O) Difference between the CESM-DPLE forecast ACCs and observational persistence. Stippling indicates that the initialized prediction is statistically significant over the observational persistence forecast at the 95% level using a *z* test. Only positive ACCs and  $\Delta$ ACCs are stippled.

### 137 **Mechanisms of pH predictability**

138 We are further interested in what lends predictability to surface pH in the CCS. We  
 139 begin by investigating predictability in the driver variables of pH: temperature, salinity,  
 140 dissolved inorganic carbon (DIC), and alkalinity. By scaling these variables to common  
 141 pH units (see supplementary for method), we can deduce which drivers aid the most in  
 142 predicting surface pH. We find that predictability in salinity-normalized DIC (sDIC) has  
 143 the largest influence on surface pH predictability over all lead years (Fig. 3C). The

144 combined predictability of both SSTs and alkalinity is roughly equivalent to sDIC over  
145 the first five lead years, while sea surface salinity plays a negligible role over all lead  
146 years (Fig. 3C). Predictability in sDIC is mainly driven by the persistence of its  
147 anomalies, but is enhanced further by initializations (Fig. S3). A budget analysis of DIC  
148 in the upper 150m of the CCS suggests that variability in vertical and lateral DIC  
149 advection plays a leading role in setting the DIC inventory, as evidenced by the high  
150 correlation between the advective flux and total tendency terms ( $r = 0.9$ ; Fig. S4).  
151 Source waters for the CCS exhibit substantial interannual to decadal variability and are  
152 mainly comprised of subarctic waters transported by the California Current (upper 200  
153 m) and eastern tropical Pacific waters transported by the California Undercurrent (200–  
154 300 m), which propagate biogeochemical anomalies into the system<sup>28,29</sup>. Thus, the  
155 subsurface and basin-wide initializations of DIC—as well as predictability of meridional  
156 and vertical transport variability—are crucial factors in making skillful multiyear  
157 predictions of surface pH variability. In turn, enhanced observations or reanalysis of  
158 these fields would be necessary for operational forecasting of surface pH in the CCS.

## 159 **Discussion**

160 While this study presents a very promising first result, there are some caveats worth  
161 noting. Simulations were run with a spatial resolution of approximately 100 km x 100  
162 km. In turn, we do not explicitly resolve the fine-scale coastal upwelling of corrosive  
163 waters (which occurs within roughly 30 km of the coastline in the CCS), but instead  
164 simulate the combined effect of coastal and curl-driven upwelling in nearshore grid cells.  
165 Our simulation also uses subgrid scale parameterizations to capture the important

166 process of eddy-induced offshore flux of tracers in the CCS<sup>30,31</sup>. Despite the coarse  
167 resolution, previous work has shown that alongshore winds, upwelling, and air-sea CO<sub>2</sub>  
168 fluxes are well-represented in this configuration of CESM relative to observations<sup>32,33</sup>. In  
169 this study, we only highlight predictability in annual averages of surface pH, since  
170 predictability at annual resolution is much higher than that of monthly resolution.  
171 However, we do find significant predictability over persistence of surface pH anomalies  
172 through June of the upwelling season following initialization, and into May of the  
173 following upwelling season (Fig. S6). Lastly, in assessing predictive skill, we are  
174 challenged by the limited coverage of gridded surface pH observations. While the  
175 observational product used in this study spans 1990–2017, the observational data for  
176 atmospheric CO<sub>2</sub> used to force the reconstruction ended in 2005, after which point a  
177 smooth scenario-based projection was used (Fig. S7A). This causes a drop-off in the  
178 ability of the reconstruction to replicate observed surface pH anomalies (Fig. S7B).  
179 Thus, we only assess skill over the 1990–2005 period, limiting our degrees of freedom  
180 for statistical significance.

181         Our results demonstrate for the first time the potential for an initialized ESM to  
182 retrospectively predict surface pH multiple years in advance in a complex, sensitive, and  
183 economically important oceanic region. Although our study highlights CESM-DPLE’s  
184 ability to predict surface pH anomalies, other ocean acidification parameters—such as  
185 calcium carbonate saturation states—can be expected to be predictable, due to their  
186 common dependence on variability in dissolved CO<sub>2</sub>. By detrending our simulated and  
187 observational products prior to analysis, we show that we have the potential to predict

188 interannual variations in surface pH. As the ocean acidification signal dominates in this  
189 region over decadal timescales, multiyear predictions of surface pH variability could aid  
190 in forecasting the acceleration or slowdown of ocean acidification in the CCS.

## 191 **Methods**

### 192 Model simulations

193 The Community Earth System Model Decadal Prediction Large Ensemble<sup>22</sup> (CESM-  
194 DPLE) is based on CESM, version 1.1, and uses the same code base, component  
195 model configurations (Table S1), and historical and projected radiative forcing as that  
196 used in its uninitialized counterpart, the CESM Large Ensemble<sup>25</sup> (CESM-LE). This  
197 includes historical radiative forcing (with volcanic aerosols) through 2005 and projected  
198 radiative forcing (including greenhouse and short-lived gases and aerosols) from 2006  
199 onward. Because CESM-DPLE and CESM-LE have an identical code base and  
200 boundary conditions, the two ensembles can be compared directly to one another to  
201 isolate the relative influence of initialization and external forcing on hindcast  
202 predictability and skill.

203 CESM-DPLE was generated via full-field initialization each year on November 1<sup>st</sup>  
204 from 1954 to 2017, for a total of 64 initialization dates<sup>22</sup>. An ensemble of 40 forecast  
205 members—created by round-off perturbations made to atmospheric initial temperature  
206 field—were integrated forward from each initialization for 122 months. The ocean and  
207 sea ice model components were initialized from a forced ocean-sea ice reconstruction  
208 (referred to as the “reconstruction”; see following section for configuration details), while  
209 atmosphere and land components were initialized from the November 1<sup>st</sup> restart files of

210 a single member of CESM-LE. In particular, the ocean biogeochemical model used in all  
211 CESM simulations in this study is the Biogeochemical Elemental Cycling (BEC) model,  
212 which contains three phytoplankton functional types (diatoms, diazotrophs, and a small  
213 calcifying phytoplankton class), explicitly simulates seawater carbonate chemistry, and  
214 tracks the cycling of C, N, P, Fe, Si, and O<sup>34,35</sup>. Note that the ocean biogeochemistry  
215 and simulated atmospheric CO<sub>2</sub> concentration are diagnostic, such that there is no  
216 feedback onto the simulated physical climate<sup>22</sup>. Further details on drift adjustment and  
217 anomaly generation can be found in the supplemental.

218 The reconstruction simulation was run from 1948–2017 with active ocean and  
219 sea ice model components from CESM, version 1.1, with identical spatial resolutions as  
220 the freely coupled CESM-DPLE and CESM-LE (Table S1). The ocean and sea ice  
221 components were forced by a modified version of the Coordinated Ocean-Ice Reference  
222 Experiment (CORE) with interannual forcing<sup>36,37</sup>, which provides momentum,  
223 freshwater, and buoyancy fluxes between the air–sea and air–ice interfaces. CORE  
224 winds were used globally, save for the tropical band (30S–30N), where NOAA  
225 Twentieth Century Reanalysis, version 2<sup>38</sup> winds (from 1948–2010) and adjusted  
226 Japanese 55-year Reanalysis Project<sup>39</sup> winds (through 2017) were used to correct a  
227 spurious trend in the zonal equatorial Pacific sea surface temperature (SST) gradient<sup>22</sup>.  
228 No direct assimilation of ocean or sea ice observations was used in the reconstruction;  
229 thus, any faithful reproduction of ocean and sea ice climatology or variability is due  
230 mainly to the atmospheric reanalysis that drives the simulation<sup>22</sup>.

231 Observational product

232 We compare initialized forecasts of surface pH to the Japanese Meteorological Agency  
233 (JMA) Ocean CO<sub>2</sub> Map product<sup>26,40</sup>, which provides monthly estimates of pH from  
234 1990–2017 over a 1° x 1° global grid. Surface pH was computed diagnostically with a  
235 carbonate system solver, using estimated surface alkalinity and pCO<sub>2</sub> as inputs. To  
236 compute gridded alkalinity, the ocean was divided into five regions, where empirical  
237 relationships were derived for *in situ* alkalinity as a function of sea surface height (SSH)  
238 and sea surface salinity<sup>26</sup> (SSS). Gridded observations of SSH and SSS (independent  
239 of the *in situ* observations) were then input into the empirical equations to derive gridded  
240 surface alkalinity. Gridded surface pCO<sub>2</sub> was computed through a multistep process.  
241 First, the ocean was divided into 44 regions and relationships between *in situ* pCO<sub>2</sub> and  
242 *in situ* SST, SSS, and Chl-*a* were derived by multiple linear regressions in each region  
243 for one to three of the variables<sup>40</sup>. The gridded pCO<sub>2</sub> product was then derived by  
244 applying these functions to independent gridded observations of SST, SSS, and Chl-*a*.  
245 Further details on the datasets used in deriving their product can be found in Takatani et  
246 al. 2014 and Iida et al. 2015.

247 Statistical analysis

248 We use deterministic metrics to compare the ensemble mean retrospective forecasts to  
249 one or both of the following baselines: (1) a persistence forecast, and (2) the  
250 uninitialized CESM-LE ensemble mean forecast. The persistence forecast of the  
251 reconstruction and observational product assumes that anomalies from each



252 initialization year persist into all following lead years<sup>41</sup>. A comparison of the initialized  
 253 forecast to the persistence forecast shows the utility of our initialized forecasting system  
 254 over a simple, low-cost forecasting method; a comparison of the initialized forecast to  
 255 the CESM-LE ensemble mean shows the utility of initializations (rather than external  
 256 forcing) in lending predictability to the variable of interest. Unless otherwise noted,  
 257 forecasts are analyzed at annual resolution. This corresponds to the January–  
 258 December average following the November 1<sup>st</sup> initialization. In turn, lead year “one” truly  
 259 covers lead months 2–14. When considering monthly predictions, lead month “one”  
 260 corresponds to the November 1<sup>st</sup>–30<sup>th</sup> average following initialization.

261 We compute the anomaly correlation coefficient (ACC) via a Pearson product-  
 262 moment correlation to quantify the linear association between predicted and target  
 263 anomalies (where the target is either the model reconstruction, CESM-LE ensemble  
 264 mean, or the observational product). If the predictions perfectly match the sign and  
 265 phase of the anomalies, the ACC has a maximum value of 1. If they are exactly out of  
 266 phase, it has a minimum value of -1. The ACC is a function of lead time<sup>11,42</sup>:

$$267 \quad ACC(\tau) = \frac{(\sum_{\alpha=1}^N (F'_{\alpha}(\tau) \times O'_{\alpha+\tau}))}{\sqrt{\sum_{\alpha=1}^N F'_{\alpha}(\tau)^2 \sum_{\alpha=1}^N O'_{\alpha+\tau}^2}}$$

268 Where  $F'$  is the forecast anomaly,  $O'$  is the verification field anomaly, and the  
 269 ACC is calculated over the period 1955–2017 (N=63) relative to the reconstruction and  
 270 CESM-LE, and over 1990–2005 (N=16 ) relative to the JMA observational product. Note  
 271 that N reduces by one for each subsequent lead year (*i.e.*, the verification window  
 272 shrinks). We quantify statistical significance in the ACC using a  $t$  test at the 95%

273 confidence level with the null hypothesis that the two time series being compared are  
274 uncorrelated. We assess statistical significance between two ACCs (*e.g.*, between that  
275 of the initialized forecast and a simple persistence forecast for the same lead time)  
276 using a z test at the 95% confidence level with the null hypothesis that the two  
277 correlation coefficients are not different.

278 To quantify the magnitude of forecast error, or the accuracy in our forecasts, we  
279 use the mean absolute error<sup>42</sup> (MAE). The MAE is 0 for perfect forecasts and increases  
280 to infinity with the amplitude of the mean absolute difference between the forecasts and  
281 target. MAE is used instead of bias metrics such as the root mean square error (RMSE),  
282 as it is a more accurate assessment of bias in climate simulations<sup>43</sup>.

$$283 \quad MAE(\tau) = \frac{1}{N} \sum_{\alpha=1}^N |F'_{\alpha}(\tau) - O'_{\alpha+\tau}|$$

284 We follow Lovenduski et al. (2019) to convert predictability in pH driver variables  
285 (SST, SSS, salinity-normalized dissolved inorganic carbon (sDIC), and salinity-  
286 normalized alkalinity (sALK)) to common pH units:

$$287 \quad r_x \cdot \frac{dpH}{dx} \cdot \sigma_x$$

288 Where  $r_x$  is the ACC between anomalies in driver variable  $x$  and target  
289 anomalies,  $\frac{dpH}{dx}$  is the linear sensitivity of pH to the driver variable, and  $\sigma_x$  is the standard  
290 deviation of driver variable anomalies in the reconstruction.

### Acknowledgements

The CESM project is supported primarily by the National Science Foundation (NSF).

This material is based upon work supported by the National Center for Atmospheric

Research, which is a major facility sponsored by the NSF under Cooperative Agreement No. 1852977. Computing and data storage resources, including the Cheyenne supercomputer (doi: 10.5065/D6RX99HX), were provided by the Computational and Information Systems Laboratory (CISL) at NCAR. The Department of Energy's Computational Science Graduate Fellowship supported RXB throughout this study (DE-FG02-97ER25308). NSL and RXB are grateful for support from the NSF (OCE-1752724). RXB acknowledges Aaron Spring for his contributions to analysis through collaborative development of the climpred package (see additional information) as well as Samantha Siedlecki, Michael Jacox, and Michael Alexander for suggestions during the analysis phase of the project.

### **Author contributions**

RXB and NSL designed the study. RXB analyzed the data, prepared figures and tables, and wrote the paper. SGY and KL coordinated and ran CESM-DPLE and FOSI simulations. NSL, SGY, MCL, and KL provided invaluable feedback throughout the study and reviewed the manuscript.

### **Additional information**

The authors of this study are unaware of any competing interests. Output from the CESM-DPLE and reconstruction can be downloaded through the Earth System Grid Federation (<https://www.earthsystemgrid.org/dataset/ucar.cgd.cesm4.CESM1-CAM5-DP.html>). The JMA Ocean CO<sub>2</sub> map product can be downloaded online at [https://www.data.jma.go.jp/gmd/kaiyou/english/co2\\_flux/co2\\_flux\\_data\\_en.html](https://www.data.jma.go.jp/gmd/kaiyou/english/co2_flux/co2_flux_data_en.html).

Analysis was performed using climpred, an open source python package developed by

the lead author for analyzing initialized forecast models. Documentation is available at <https://climpred.readthedocs.io>. Post-processed model output and observations as well as Jupyter notebooks used to create all figures in this study will be made available by the lead author on Zenodo and Github following acceptance and publication of this manuscript.

## References

1. Doney, S. C., Fabry, V. J., Feely, R. A. & Kleypas, J. A. Ocean acidification: The other CO<sub>2</sub> problem. *Annu. Rev. Mar. Sci.* **1**, 169–192 (2009).
2. Gruber, N. *et al.* Rapid progression of ocean acidification in the California Current System. *Science* **337**, 220–223 (2012).
3. Huyer, A. Coastal upwelling in the California Current System. *Prog. Oceanogr.* **12**, 259–284 (1983).
4. Pauly, D. & Christensen, V. Primary production required to sustain global fisheries. *Nature* **374**, 255–257 (1995).
5. Feely, R. A., Sabine, C. L., Hernandez-Ayon, J. M., Ianson, D. & Hales, B. Evidence for upwelling of corrosive ‘acidified’ water onto the continental shelf. *Science* **320**, 1490–1492 (2008).
6. Bednaršek, N. *et al.* *Limacina helicina* shell dissolution as an indicator of declining habitat suitability owing to ocean acidification in the California Current Ecosystem. *Proc R Soc B* **281**, 20140123 (2014).

7. Bednaršek, N. *et al.* Exposure history determines pteropod vulnerability to ocean acidification along the US West Coast. *Sci. Rep.* **7**, (2017).
8. Fisheries economics of the United States 2015. (2017).
9. Clements, J. C. & Chopin, T. Ocean acidification and marine aquaculture in North America: potential impacts and mitigation strategies. *Rev. Aquac.* **9**, 326–341 (2017).
10. Jacox, M. G., Alexander, M. A., Stock, C. A. & Hervieux, G. On the skill of seasonal sea surface temperature forecasts in the California Current System and its connection to ENSO variability. *Clim. Dyn.* (2017). doi:10.1007/s00382-017-3608-y
11. Hervieux, G. *et al.* More reliable coastal SST forecasts from the North American multimodel ensemble. *Clim. Dyn.* (2017). doi:10.1007/s00382-017-3652-7
12. Stock, C. A. *et al.* Seasonal sea surface temperature anomaly prediction for coastal ecosystems. *Prog. Oceanogr.* **137**, 219–236 (2015).
13. Siedlecki, S. A. *et al.* Experiments with seasonal forecasts of ocean conditions for the Northern region of the California Current upwelling system. *Sci. Rep.* **6**, (2016).
14. Park, J.-Y., Stock, C. A., Dunne, J. P., Yang, X. & Rosati, A. Seasonal to multiannual marine ecosystem prediction with a global Earth system model. *Science* **365**, 284–288 (2019).
15. Tommasi, D. *et al.* Managing living marine resources in a dynamic environment: The role of seasonal to decadal climate forecasts. *Prog. Oceanogr.* **152**, 15–49 (2017).
16. Seferian, R. *et al.* Multiyear predictability of tropical marine productivity. *Proc. Natl. Acad. Sci.* **111**, 11646–11651 (2014).

17. Li, H., Ilyina, T., Müller, W. A. & Sienz, F. Decadal predictions of the North Atlantic CO<sub>2</sub> uptake. *Nat. Commun.* **7**, (2016).
18. Séférian, R., Berthet, S. & Chevallier, M. Assessing the decadal predictability of land and ocean carbon uptake. *Geophys. Res. Lett.* **45**, 2455–2466 (2018).
19. Lovenduski, N. S., Yeager, S. G., Lindsay, K. & Long, M. C. Predicting near-term variability in ocean carbon uptake. *Earth Syst. Dyn.* **10**, 45–57 (2019).
20. Li, H., Ilyina, T., Müller, W. A. & Landschützer, P. Predicting the variable ocean carbon sink. *Sci. Adv.* **5**, eaav6471 (2019).
21. Bonan, G. B. & Doney, S. C. Climate, ecosystems, and planetary futures: The challenge to predict life in Earth system models. *Science* **359**, eaam8328 (2018).
22. Yeager, S. G. *et al.* Predicting Near-term changes in the Earth system: A large ensemble of initialized decadal prediction simulations using the Community Earth System Model. *Bull. Am. Meteorol. Soc.* **99**, 1867–1886 (2018).
23. Meehl, G. A. *et al.* Decadal climate prediction: An update from the trenches. *Bull. Am. Meteorol. Soc.* **95**, 243–267 (2014).
24. Branstator, G. & Teng, H. Two limits of initial-value decadal predictability in a CGCM. *J. Clim.* **23**, 6292–6311 (2010).
25. Kay, J. E. *et al.* The Community Earth System Model (CESM) large ensemble project: A community resource for studying climate change in the presence of internal climate variability. *Bull. Am. Meteorol. Soc.* **96**, 1333–1349 (2015).

26. Takatani, Y. *et al.* Relationships between total alkalinity in surface water and sea surface dynamic height in the Pacific Ocean. *J. Geophys. Res. Oceans* **119**, 2806–2814 (2014).
27. Iida, Y. *et al.* Trends in pCO<sub>2</sub> and sea–air CO<sub>2</sub> flux over the global open oceans for the last two decades. *J. Oceanogr.* **71**, 637–661 (2015).
28. Pozo Buil, M. & Di Lorenzo, E. Decadal dynamics and predictability of oxygen and subsurface tracers in the California Current System. *Geophys. Res. Lett.* **44**, 4204–4213 (2017).
29. Bograd, S. J., Schroeder, I. D. & Jacox, M. G. A water mass history of the Southern California Current System. *Geophys. Res. Lett.* 2019GL082685 (2019).  
doi:10.1029/2019GL082685
30. Gent, P. R. & McWilliams, J. C. Isopycnal mixing in Ocean Circulation Models. *J. Phys. Oceanogr.* **20**, 150–155 (1990).
31. Gruber, N. *et al.* Eddy-induced reduction of biological production in eastern boundary upwelling systems. *Nat. Geosci.* **4**, 787–792 (2011).
32. Brady, R. X., Alexander, M. A., Lovenduski, N. S. & Rykaczewski, R. R. Emergent anthropogenic trends in California Current upwelling. *Geophys. Res. Lett.* **44**, 2017GL072945 (2017).
33. Brady, R. X., Lovenduski, N. S., Alexander, M. A., Jacox, M. & Gruber, N. On the role of climate modes in modulating the air–sea CO<sub>2</sub> fluxes in eastern boundary upwelling systems. *Biogeosciences* **16**, 329–346 (2019).

34. Moore, J. K., Lindsay, K., Doney, S. C., Long, M. C. & Misumi, K. Marine ecosystem dynamics and biogeochemical cycling in the Community Earth System Model [CESM1(BGC)]: Comparison of the 1990s with the 2090s under the RCP4.5 and RCP8.5 scenarios. *J. Clim.* **26**, 9291–9312 (2013).
35. Lindsay, K. *et al.* Preindustrial-control and twentieth-century carbon cycle experiments with the Earth system model CESM1(BGC). *J. Clim.* **27**, 8981–9005 (2014).
36. Griffies, S. M. *et al.* Coordinated Ocean-ice Reference Experiments (COREs). *Ocean Model.* **26**, 1–46 (2009).
37. Large, W. G. & Yeager, S. G. The global climatology of an interannually varying air–sea flux data set. *Clim. Dyn.* **33**, 341–364 (2009).
38. Compo, G. P. *et al.* The Twentieth Century Reanalysis Project. *Q. J. R. Meteorol. Soc.* **137**, 1–28 (2011).
39. Tsujino, H. *et al.* JRA-55 based surface dataset for driving ocean–sea-ice models (JRA55-do). *Ocean Model.* **130**, 79–139 (2018).
40. Iida, Y. *et al.* Trends in pCO<sub>2</sub> and sea–air CO<sub>2</sub> flux over the global open oceans for the last two decades. *J. Oceanogr.* **71**, 637–661 (2015).
41. Van den Dool, H., CPC, P. S. & others. *Empirical methods in short-term climate prediction*. (Oxford University Press, 2007).
42. Jolliffe, I. T. & Stephenson, D. B. *Forecast verification: a practitioner’s guide in atmospheric science*. (John Wiley & Sons, 2012).



43. Willmott, C. & Matsuura, K. Advantages of the mean absolute error (MAE) over the root mean square error (RMSE) in assessing average model performance. *Clim. Res.* **30**, 79–82 (2005).